Powder Technology 281 (2015) 76–82

Contents lists available at ScienceDirect

Powder Technology

journal homepage: www.elsevier.com/locate/powtec

Aerosol manipulation by acoustic tunable phase-control at resonant frequency

Zhenghui Qiao [a], Yaji Huang [a], Naso Vincenzo [b], Wei Dong [a,b,*]

[a] Key Laboratory of Energy Thermal Conversion and Control of Ministry of Education, School of Energy & Environment, Southeast University, Nanjing 210096, PR China
[b] Interuniversity Research Centre on Sustainable Development, SAPIENZA University of Rome, Via Cavour, 256-00184 Rome, Italy

ARTICLE INFO

Article history:
Received 29 December 2014
Received in revised form 3 April 2015
Accepted 30 April 2015
Available online 9 May 2015

Keywords:
Phase-control
Interaction
Aerosols
Acoustic field
Nonuniform
Resonance

ABSTRACT

The aerosols regularly manipulated by modular platform of acoustic tunable phase-control at resonant frequency 2.6427 kHz are demonstrated in this paper. In order to make full of the superimposition of multiple waves in non-uniform two dimension acoustic standing wave field, the modular platform is composed of the square cavity and the two pairs of symmetric acoustic sources with Helmholtz resonators. The modular platform allows that the effective volume of cavity is 32.8 (length) × 32.8 (width) × 5 (height) cm^3 and also the tunable acoustic phase-control is realized by proposed two different phase modes named π-mode phase and 0-mode phase. The ranges of the aerosol size distribution and the aerosol concentration are 0.08 μm–1 μm and 51.6–93.3% (Opacity), respectively. The experimental temperature remains at 298 K. Results indicate that the platform causes perfect nonuniform two-dimension acoustic standing wave field. Under the condition of π-mode phase, the manipulation is better than that under 0-mode phase; the characteristic length of X-pattern for displaying the manipulation is half-wavelength larger than quarter-wavelength acquired in one-dimension acoustic standing wave field. The major areas to remove aerosols are 39 cm^2 under π-mode phase and 9.7 cm^2 under 0-mode phase. The phase is an important parameter for impacting the manipulation of aerosols. For explaining the difference of manipulation under the two phase conditions, the relative structural factors of acoustic field are found and considered as the intermediate variables from acoustic tunable phase to aerosol manipulation. Especially, the large neck for the shape of sound pressure nodes might cause weak interaction between aerosols and acoustic field and further result in the unexhaustive manipulation.

1. Introduction

Aerosol manipulation in acoustic standing wave (ASW) field can achieve the regular motion of aerosols in a finite space. This regular motion plays the significant role in the process of aerosol removal.

Recently, there are different experiments to study the aerosol behaviors in ASW field, in order to manipulate the aerosol removal more efficiently [1–5]. Frequency and sound pressure as the important characteristic parameters of ASW field have been verified acting as the significant factors to impact the effect of an acoustic field on aerosol manipulation. Enough high sound pressure (140 dB [1], 120 dB [3]) and appropriate frequency (1.4 kHz [1], 1.416 kHz [3]) are essential to acquire an obvious manipulation effect. However, the study on the aerosol manipulation by the phase acting as one characteristic parameter of ASW field is rare, which is one objective of this paper.

In the aspects of particle manipulation by ASW about phase within liquid (water [6,7] generally selected), the significant study on the phase-control has been done currently. One thing they [6,7] mostly focused on is the microscopic scale of set-up such as micro-channel. Besides, Raeymaekers et al. [8] studied the macro scale patterns [8] about particle manipulation using bulk acoustic wave in water. However, the physical characters of particle environment for liquid and gas respectively are obviously different such as the acoustic velocity, the viscosity, the density, etc. At the same time, the acoustic source is a piezoelectric transducer for producing high frequency (740 kHz [6], 91 MHz [7]) acoustic wave in water. Utilizing the plate [6,8] and the cylinder [8] for the types of conventional piezoelectric transducer can transmit directly satisfactory acoustic wave into water. Conversely, when used to manipulate particles in air, the conventional piezoelectric transducer needs to be improved based on the acoustic impedance match between transducer and air, for example the additional radiation plate and mechanical amplifier used in the device of Juan et al. [4]. Therefore, without special improvement for the device, the conventional acoustic source cannot produce enough high sound pressure used for aerosol manipulation at the relative low frequency like 1.4 kHz in air medium.

Other relative important researches are the acoustic manipulation [9] and levitation [10–12] of micro- and macro scale particles in gas. Karpul et al. [9] designed industrial acoustic filters to manipulate

* Corresponding author at: Key Laboratory of Energy Thermal Conversion and Control of Ministry of Education, School of Energy & Environment, Southeast University, Nanjing 210096, PR China. Tel.: +86 13851779962.
E-mail address: dongwei59@seu.edu.cn (W. Dong).

http://dx.doi.org/10.1016/j.powtec.2015.04.081
0032-5910/

particles, and showed the advantage of optimizing operating and structure factors of acoustic filter on achieving better manipulation. They studied respectively two kinds of different particles, radiuses of 1 μm for graphite and 1 mm for polystyrene foam. Weber et al. [10] constructed an acoustic levitator to achieve levitating liquids at resonant frequency ~22 kHz. Their particle diameter is in the range of 1–3 mm. Daniele et al. [11] designed an acoustic macro platform for levitating a steel sphere of 5 mm in air using ASW of 25 kHz. Therefore, it is appropriate that we study the effect of the phase of ASW on the aerosol manipulation at low resonant frequency, especially in macroscopic cavity. In terms of the industrial occasions for flue gas emission from coal and oil combustion, the amount of emission for aerosols is usually huge [13]. When applying the aerosol manipulation in ASW field to remove aerosols in these occasions, the design and manufacture of the huge cavity to achieve optimal acoustic resonance is also the one of challenges.

On the other hand, among the current studies, one dimension ASW field is prior selected for the establishment of ASW field by one acoustic source and reflective plate [4,14] or by two symmetric acoustic sources [15,16]. However, two-dimension ASW field has potential advantage making full of the superimposition of multiple waves and such research has been developed. In some studies [4,6,17] the two-dimension ASW field is formally two dimensional in space, but such ASW field can be equal to one dimension ASW field because of the uniform distribution along the direction perpendicular to the propagation of acoustic wave. In fact, such two-dimension is only the extension of one dimension ASW field in plane, and it still belongs to the scope of one-dimension in nature. In contrast, the nonuniform two-dimensional ASW field (NTASWF) is rarely used for aerosol manipulation, which is another objective of this paper.

When carrying out the aerosol manipulation in NTSAWF, however, how to control the interaction between aerosols and two dimension ASW field becomes a significant topic on the interaction between aerosols and acoustic field environment of their existing. This paper demonstrates that the aerosol moving behavior can be regularly manipulated by modular platform of acoustic tunable phase-control in NTASWF at 2.6427 kHz of a low frequency.

2. Experiment and method

2.1. Experimental set-up

The modular platform of acoustic tunable phase-control consists of two types of modules, one horizontal square cavity and two pairs of symmetric acoustic sources, showed by Fig. 1. The square cavity is made up of Perspex plate of thickness 5 mm and its volume is 32.8 (length) × 32.8 (width) × 5 (height) cm^3. Four same power acoustic transducers are arranged on the four sides symmetrically against to the center point of square cavity. Two acoustic transducers of each pair are opposing each other, and constitute symmetric acoustic sources of a pair with respect to the center point. These acoustic sources have same center frequency. The acoustic source is the type of acoustic streaming, named as Helmholtz resonator source (HRS) [16,18]. Helmholtz resonator source is composed of electromagnetic speaker and Helmholtz resonator. HRS operating at Helmholtz resonance frequency (HRF) can produce great acoustic wave of similar single frequency [18]. Such acoustic wave can satisfy the requirement of sound pressure when manipulating aerosols by acoustic tunable phase-control. In order to realize the resonance of modular platform and cause suitable NTASWF, the working frequency of acoustic source is equal to the HRF and to the five order harmonic frequency of square cavity.

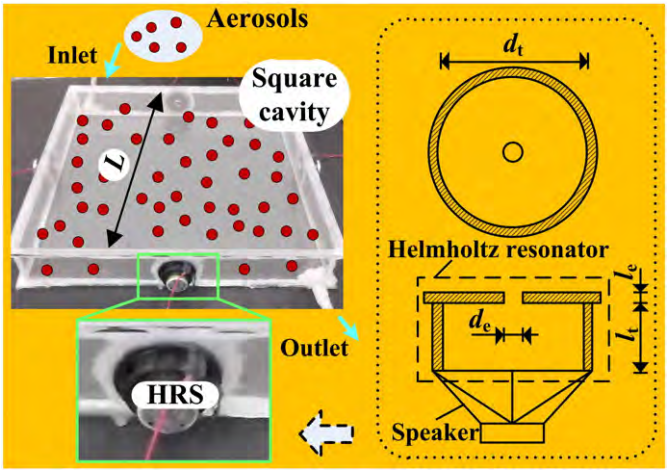

Fig. 1. Schematic diagram of setup.

The structural parameters of modular platform satisfied the following formula [16,19]

$$(nc/(2L))^2 = (c^2/4\pi^2)\left(\pi d_e^2/4\right)/(l_e + 0.73d_e)/\left(l_t\pi d_t^2/4\right) = f^2, \quad (1)$$

where $n = 5$ is the five order harmonic order of square cavity; L is the length of square cavity; c is the acoustic velocity of air; $d_e = 8$ mm, $l_e = 5$ mm, $d_t = 35$ mm & $l_t = 2$ mm are the geometric parameters of Helmholtz resonator; and f is HRF equal to 2.6427 kHz in our study, and equals the center frequency of acoustic source.

Eq. (1) is a similarity condition for resonance. According to this similarity condition, the geometric size (length and width) of the square cavity can be larger. For example, a smaller f, satisfying the geometric parameters d_e, l_e, d_t, l_t, corresponds to a longer L, or an appropriate larger n, satisfying the positive odd integer (the even integer has not been verified [16]), corresponds to a longer L. In order to avoid the generation of the ASW field in the direction of height, the height of square should also be less than half-wavelength. This constraint ensures the production of NTASWF only in the plane of length–width. Therefore, under the constraint of Eq. (1) and the height constraint, the influence of the setup dimension amplified on acoustic tunable phase-control can be neglected [16]. It must be pointed out that such method has not been suggested in previous study.

The sound pressure, p, radiated from the acoustic sources is $p_m^\varepsilon = p_a \exp(i(\omega t + \psi_m^\varepsilon))$, here, p_a and ω are respectively the amplitude and angular frequency of sound pressure, t is the time, the phase $\psi = \pi$ or 0 represents the contrary (π) and same (0) to the vibration directions of the symmetric acoustic sources (note that using the inversion of the two vibration directions [16] does not produce the general phase achieved by Kun et al. [20], and the study on how to improve the method to achieve the general phase for our proposed set-up has not been carried out), the subscript $m = 1$ or 2 represents the two sources of the each pair of symmetric acoustic sources, the superscript $\varepsilon = 1$ or 2 represents the two pairs. Acoustic tunable phase-control can be realized through the tunability of contrary and same phase between acoustic waves radiated from the each pair of symmetric acoustic sources. Therefore, the acoustic tunable phase-control in this paper is equivalent to two different phase modes, π-mode phase and 0-mode phase. The foundation of this classification is based on the tunability for the phase of the each pair of symmetric acoustic sources [16]. Using the phase of ψ_m^ε, the two modes can be expressed as

$$\begin{bmatrix} (\psi_m^\varepsilon)_{\pi\text{-mode}} \\ (\psi_m^\varepsilon)_{0\text{-mode}} \end{bmatrix} = \begin{bmatrix} \left(\left(\psi_m^1\right), \left(\psi_m^2\right)\right)_{\pi\text{-mode}} \\ \left(\left(\psi_m^1\right), \left(\psi_m^2\right)\right)_{0\text{-mode}} \end{bmatrix} = \begin{bmatrix} (0,\pi), (\pi,0) \\ (0,0), (0,0) \end{bmatrix}. \quad (2)$$

It must be pointed out that according to the right side of Eq. (2), there also have other modes, such as [(0, π), (π, 0)], [(π, π), (π, π)], [(0, π), (0, 0)]. Due to the symmetry of square cavity, [(0, π), (π, 0)] and [(π, π), (π, π)] is the same as [(0, π), (π, 0)] and [(0, 0), (0, 0)],

respectively. The mode of [(0, π), (0, 0)] is derived from the difference between two pairs. Study on the mode difference between several pairs is not referred in this paper.

A sinusoidal AC voltage signal at amplitude 15 V and frequency 2.6427 kHz is input electromagnetic speaker by an amplifier, and the peak sound pressure amplitude resulted in ASW field is 108 Pa. The voltage amplitude used by us is the same as Teruyuki et al. [21], but the frequency is far lower than 1.75 MHz, which used by them. Tobacco smoke is filled into the square cavity so as to display manipulating performance of the acoustic tunable phase-control on aerosols. The aerosol size is less than 1 μm [22]. The aerosol size distribution to aerosols larger than 50% is covered in 0.08–1 μm [22,23] (0.08–0.7 μm [22], 0.25–1 μm [23]). The quantitative aerosol concentration can be demonstrated with opacity [24–26] 51.6–93.3% (measured by opacity smoke meter (SV-5Y) and exhaust gas analyzer (SV-5Q), high opacity corresponding to high aerosol concentration), and the components corresponding contain NO_x(53–56 ppm), HC (467–664 ppm), CO (1.27–1.59%), CO_2 (3.58–4.32%), and O_2 (17.2–20.69%). The experimental temperature is kept at the uniform ambient temperature of 298 K.

2.2. Analysis method

2.2.1. Acoustic radiation force

A number of papers [6,7,11,12,17,21,27–30] on particle manipulation using ASW have indicated that aerosols in ASW field are exerted an external acoustic radiation force. The acoustic radiation force results from the acoustic radiation pressure [11,31]. Due to the size 0.08–1 μm of aerosols and the wavelength 13.12 cm of acoustic wave in our experiment, the regime of aerosol manipulation using ASW agrees with the Rayleigh regime [6]. Because the size of aerosols used by us is much smaller than the wavelength of acoustic wave [12], once the shape of aerosols is equivalent to compressible sphere, the acoustic radiation force, F, on a single, small sphere can be given by Gor'kov [28].

$$F = -\left(4\pi R^3/3\right)\nabla\left(p_A^2/(4\rho_0 c_0^2) f_1 - 3\rho_0 v_A^2/8 f_2\right), \tag{3a}$$

$$f_1 = \left(1-\rho_0 c_0^2/(\rho c^2)\right), \tag{3b}$$

$$f_2 = 2(\rho-\rho_0)/(2\rho+\rho_0), \tag{3c}$$

where, R is the equivalent radius of aerosols, p_A and v_A are the pressure amplitude and the velocity amplitude in ASW, ρ_0 and c_0 are the density and the acoustic velocity of the aerosols, f_1 and f_2 are the acoustic contrast factors, ρ and c are the density and the acoustic velocity of the host fluid medium. According to the theory of Gorkov, Eq. (3a)–(3c) can be used in any ASW field except for the traveling wave field [17,28].

Under the effect of such external force, the aerosols in the host fluid medium can be manipulated between sound pressure nodes and anti-nodes [21,27]. ρ_0, c_0, ρ, c are the key parameters to determine the aerosols are driven to pressure nodes or anti-nodes [11,29]. In order to distinguish the direction of the driven using one parameter, J. Greenhall et al. [6] used the improved acoustic contrast factor [29,30], Φ,

$$\Phi = (5\rho_0 - 2\rho)/(2\rho_0 + \rho) - \beta_0/\beta \tag{4}$$

where, β_0 and β are the compressibility of the aerosols and the host fluid medium, respectively.

If $\Phi > 0$, the aerosols are driven to the nearest pressure nodes. If $\Phi < 0$, the aerosols are driven to the nearest pressure anti-nodes [6,9].

2.2.2. The effect of temperature

According to the mechanism of Brownian motion [32,33], the aerosols for the particle diameter size at submicron are driven to take irregular motion at a given ambient temperature as 298 K [34]. In a given space, the temperature gradient [35] will cause the different kinetic energies for the aerosols [33]. The numerous aerosols with different kinetic energies will then make the number-mean motion directional [33] from the high temperature positions to the low temperature positions. However, due to the uniform ambient temperature in our experiment, the difference of temperature at different positions can be neglected. The aerosol number distribution, affected by the temperature gradient, over different positions is neglected. Meanwhile, the effect of temperature changing with time can also be neglected due to the constant experiment temperature [32].

2.2.3. The selection of characteristic parameters

According to Section 2.2.1, aerosol manipulation in NTASWF is determined by the characteristics of acoustic field, such as the distribution of sound pressure in the square cavity. Other characteristics contain the value of sound pressure and the frequency, because they decide firstly whether the aerosol manipulation is realized or not [1,3]. On the other hand, the distribution of sound pressure presents the positions of pressure anti-nodes and pressure nodes, and these anti-nodes and nodes present the positions of aerosols under the realization of aerosol manipulation. Consequently under the conditions of the realization, that is, at the appropriate sound pressure and frequency, we focus on the aerosol number distribution for the two modes. The distribution of sound pressure can be used to study the relation between acoustic tunable phase-control and aerosol manipulation.

2.2.4. The analysis of NTASWF

In the previous papers [6,20,36], the acoustic reflection was considered as an unfavorable [20,36] phenomena accompanied. The authors [6,20,36] took measures to reduce the effect of the reflection of sides on acoustic field. Conversely, we consider the effect of reflection and therefore, the structure of NTASWF is complex [6]. According to the symmetry of NTASWF in our set-up, the study to the characteristic of acoustic field is simplified as the pressure variation with the positions covered in the two-dimension region of one eighth of square. Test points arranged, x_1, x_2, x_3, x_4, x_5, x_6, x_7, x_8, x_9, x_{10}, x_{11} are showed in Fig. 2. The distance between contiguous two test points for x_1, x_2, x_3, x_4, x_5, and x_6 and for x_1, x_7, x_8, and x_9 equals to quarter-wavelength. x_6, x_{10}, and x_{11} cross the diagonal line of square.

The wave equation for sound pressure p in NTASWF is identified with the Helmholtz equation.

$$\nabla^2 p + k^2 p = 0 \tag{5}$$

where $\nabla^2 = \partial/\partial x^2 + \partial/\partial y^2$ is the Laplace operator for the plane coordinate x–y; k is the wave number.

It is well known that Eq. (5) belongs to the Laplace equation. The internal acoustic sources mounted symmetrically on four sides of square cavity constitute a closed and solved physical system. The Laplace

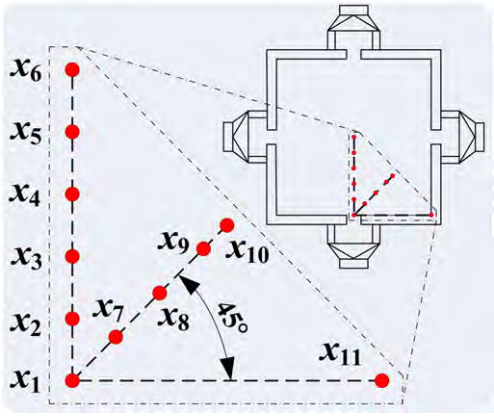

Fig. 2. Arrangement for the test points.

equation model based on such physical system is solved. Eq. (2) gives out the boundary conditions at the positions of acoustic sources for the two modes.

In addition, Eq. (5) indicates that the second derivative of sound pressure $\nabla^2 p$ is existent in NTASWF. According to the definition of spline interpolation function, the fitted curves based on spline interpolation function for the sound pressure magnitudes at the arranged positions demonstrate the changed regulations of sound pressure with continuous positions. By comparing the changed regulations of sound pressure between under π-mode phase and under 0-mode phase, the effect of acoustic tunable phase-control on aerosol manipulation can be analyzed.

3. Analysis and discussion

3.1. Performance of aerosol manipulation

In Fig. 3, the regions of X, B_{I}, B_{II}, B_{III} & B_{IV} divided out by the curved dotted lines represent the aerosol characteristic number distributions for types of five based on the five regions, which demonstrates the distribution characteristic of aerosol concentration in the square cavity under the two modes. The regions of C represent the gathered aerosols in the region of X. The dark region of X represents the concentration of aerosols in this region, which is low. The bright regions within the regions of B represent the concentration of aerosols in the regions, which is high. Note that the dark regions in the regions of B are due to the lack of background light, and their concentrations of aerosols are actually similar to bright regions. Half-wavelength of acoustic wave, $\lambda/2$, is the characteristic length used for representing the size of region X. This characteristic length represents the major size of region X.

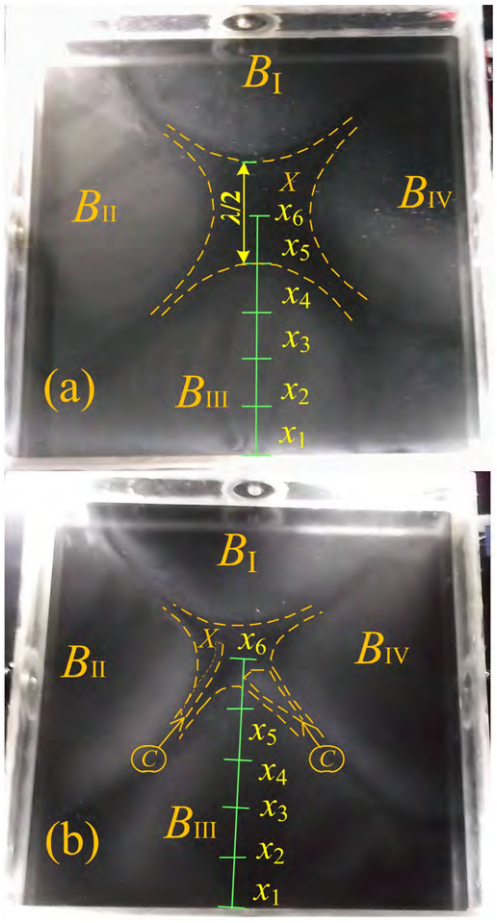

Fig. 3. Effect of NTASWF on aerosol manipulation. (a), π-mode phase. (b), 0-mode phase.

Fig. 3 shows that aerosols in square cavity are obviously divided into five regions by acoustic field. These regions constitute an X-pattern, no matter whether for π-mode phase or for 0-mode phase. On the basis of the NTASWF under the two modes, the aerosols are directional driven between nodes and anti-nodes. Under the remaining action of acoustic radiation force, the aerosols within region X are removed to other four regions, and accumulated these places. Therefore, aerosols within region X are few, contrary to the numerous aerosols in other four regions of B. In this region X, aerosols are interestingly removed away. Such removal indicates that the fundamental principle of set-up might be used to regional aerosol removal in the space scale of cm-level, $32.8 \times 32.8 \times 5\ \mathrm{cm}^3$, such as in specific room or workplace with massive aerosols. In contrast, for other four regions, aerosols are gathered to these four places. Such gathering indicates that the fundamental principle of set-up might achieve aerosol aggregation in somewhat macro space and apply to the separation of component of aerosols. In other words, the application range potential includes the places where require controlling concentration distribution for aerosols.

Meanwhile, it is noteworthy that the X-pattern is well agreed with the recent important numerical result of Ding et al. [27] without regard of their liquid medium experiment, the significant difference compared to gas in our current study. Besides, in terms of the size of X-pattern, something of interest in our study is that the size of X-pattern is cm-level much larger than mm-level of Ding, $2.5 \times 2.5 \times 3.5\ \mathrm{mm}^3$. This is mainly because our set-up is effective at a lower resonance frequency (2.6427 kHz) rather than several or more dozens of thousand hertz due to the acoustic impedance difference. According to $\lambda = c/f$, this frequency causes a longer wavelength. This wavelength corresponds to a bigger wavelength space containing more aerosols. Then, the numerous aerosols can be simultaneously manipulated within the bigger wavelength space. Therefore, our technology might have the advantage of convenient implement for the simultaneous manipulation of numerous environmental aerosols.

In addition, in terms of the effectiveness of aerosol manipulation in space, the characteristic length under π-mode phase is 6.56 cm equal to half-wavelength. That under 0-mode phase is ~3.28 cm equal to quarter-wavelength. It is obvious that the size of region X under π-mode phase is much larger than that under 0-mode phase. This large size verifies the manipulative effectiveness under π-mode phase. Furthermore, seeing from Fig. 3(b), under 0-mode phase there are two specific remaining existences of gathered aerosol regions of C embedded in region X. These remaining existences indicate that the manipulation of aerosols in region X is not exhaustive under 0-mode phase. Accordingly, the performance of absolute manipulation under π-mode phase is also better than that under 0-mode phase.

3.2. Acoustic tunable phase-control

According to Eq. (2), the acoustic tunable phase-control is carried out by providing the boundary conditions on the acoustic sources of NTASWF. According to Eq. (5), under the effect of the boundary conditions the NTASWF is caused under π-mode phase and 0-mode phase. According to Eqs. (3a)–(3c) & (4), the NTASWF corresponding determine the manipulation of aerosols between nodes and anti-nodes. Therefore, the realization of acoustic tunable phase-control contains the establishment of NTASWF by the two different modes, and the aerosol manipulation based on the NTASWF.

3.2.1. Establishment of NTASWF

After defining time-phase $\chi = i\omega t$ or $\chi = i\omega t + \pi$, the periodic changing of sound pressure with time, $p(t) \sim \exp(i\chi)$, is demonstrated by the circulated repeat of sound pressure over the time-phase of 2π, showed by Fig. 4(a). The optional test positions are based on where able to achieve peak sound pressure under the two modes. The sound pressure magnitude data in greater than two cycles is dispersed in Fig. 4(a), varied with different time-phase. The dispersed data in

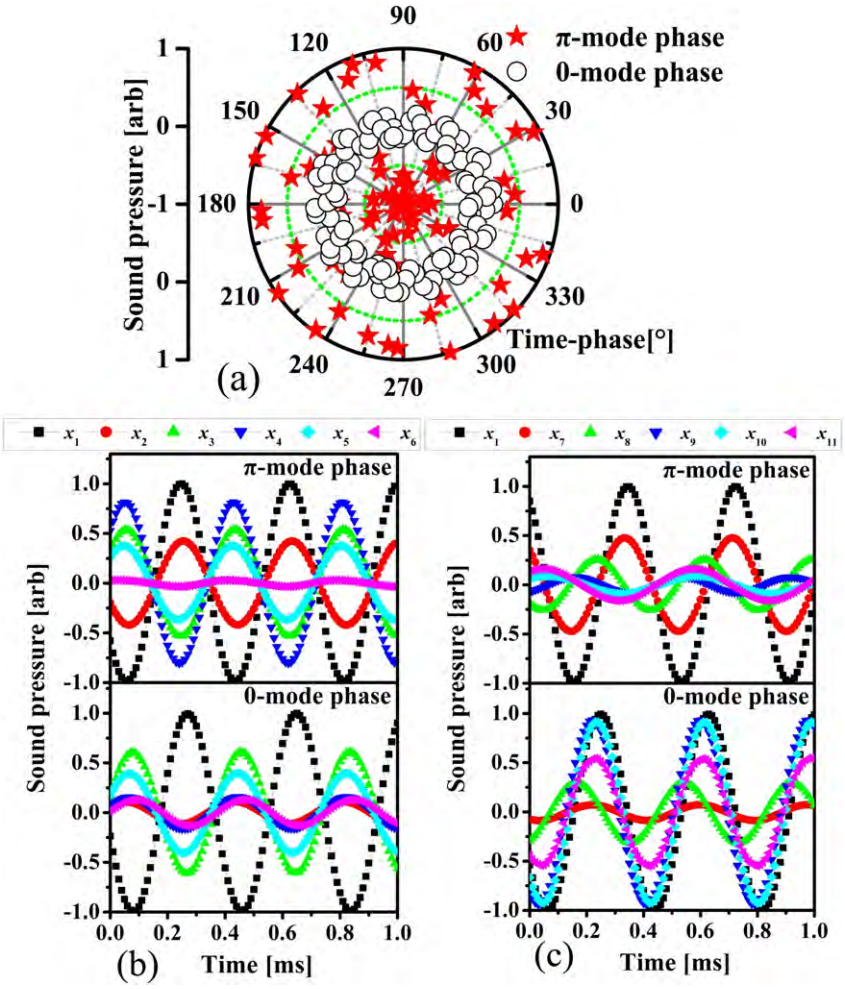

Fig. 4. Peak sound pressure (a) and time evolution of sound pressure (b) & (c).

Fig. 4(a) indicates that the sound pressure changing under π-mode phase is more drastic than that under 0-mode phase. The amplitude of sound pressure under π-mode phase is ~6 times larger than that under 0-mode phase.

In addition, Fig. 4(b) & (c) shows that the sound pressure varying with time is nonuniform in the region of one eighth of square, which indicates the production of NTASWF under the two modes.

3.2.2. Relation between NTASWF and aerosol manipulation

Base on the size of region *X* showed in Fig. 3, the square of characteristic length (λ/2) is the major area of region *X* in which the concentration of aerosols is low. The areas, $6.25^2 \approx 39$ cm^2 (π-mode) and $3.12^2 \approx 9.7$ cm^2 (0-mode), approximately represent the areas in which using NTASWF remove aerosols. Further, such two areas show directly the performance of aerosol manipulation in the NTASWF. Consequently, studying the acoustic field along the characteristic length instead of the whole one eighth region of square showed in Fig. 2 satisfies the requirement for exploring the relation between NTASWF and aerosol manipulation. In other words, it is appropriate that using the sound pressure distribution passing x_1, x_2, x_3, x_4, x_5 & x_6 analyzes the relationship between acoustic tunable phase-control and aerosol manipulation.

In Fig. 5, asterisk 1 represents test point. Solid line 2 represents fitted curve based on the cubic spline interpolation function using these test points. Short dash line 3 indicates the linear interpolation used to

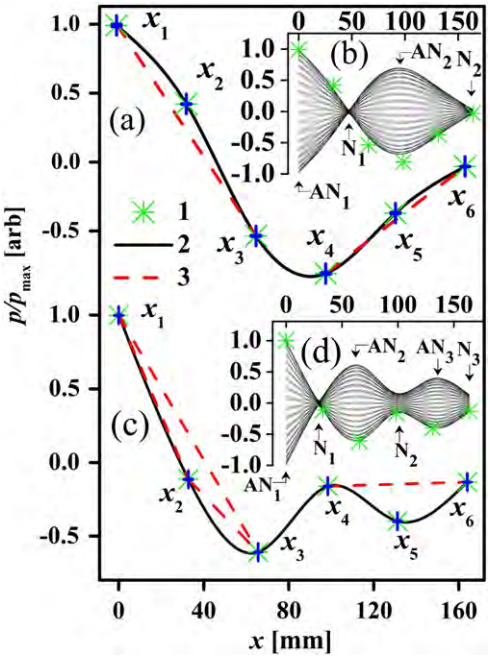

Fig. 5. Sound pressure distributions. (a) & (b), π-mode phase. (c) & (d), 0-mode phase.

judge the changing trend of solid line along *x*-axis. The patterns in (b) & (d) represent sound pressure distributions in more than one cycle using the same fitting method. The pressure node & anti-node are abbreviated to N & AN.

Fig. 5 demonstrates the sound pressure distributions. The fluctuation of sound pressure is different along the characteristic length. In terms of π-mode phase and 0-mode phase the changing trends of pressure along *x*-axis in ASW field are almost contrary. This contrary is based on the difference between the two types of fitted curves. These contrary trends indicate that, just as showed by Fig. 5(b), under π-mode phase there are respectively two pressure anti-nodes and two pressure nodes along *x*-axis. Under 0-mode phase, the quantities corresponding to anti-nodes and nodes are three, showed by Fig. 5(d). As the consequence, the intensity distribution of pressure variation along *x*-axis under 0-mode phase is more disperse than that under π-mode phase. Since aerosols in ASW field are limited in each region between contiguous anti-node and node (see Section 2.2.1), that more disperse distribution can directly bring about the more disperse number distribution of aerosols, just as the experimental existence of the regions of *C* under 0-mode phase.

According to Fig. 5(b) & (d), the sound pressure distribution curves varied from time shape sole pattern symmetrically against to itself horizontal symmetric line. Under π-mode phase the sound pressure variation from position x_4 to position x_6 is alternatively monotonic increase or decrease and does not cross zero point. The increase and the decrease correspond to the moments when the sound pressure distribution curves are respectively below and above the symmetric line. There is not an extreme value at x_5 like that under 0-mode phase. Such variation under π-mode phase might be one reason of region *X* of size greater than that under 0-mode phase. Additionally, the external profile of the sole pattern has two boundary curves in the up and down. The curvature of the two curves determines the curvature of sound pressure distribution curve at each moment, defined as the curvature of shaped pattern. The difference of the pattern curvature of pressure distribution under the two modes might also be one reason of that. Under π-mode phase the position x_5 becomes an inflection point and the corresponding sound pressure does not equal to zero. Such two reasons probably result in the absolute removal of aerosols in region *X*.

In particular, according to Fig. 5(b) & (d), as sound pressure distribution varies from different moments, there leads to two types of pressure nodes, neck and dot. The sound pressure node dots under 0-mode phase are not similar to that under π-mode phase, and large necks lead to the weak interactions between acoustic fields and aerosols. The weak interactions might also result in the aerosols remaining existence of regions of *C*. It must be pointed out that the large neck causes high peak sound pressure at node and low pressure gradient between contiguous node and anti-node. Therefore, according to Section 2.2.1, the acoustic radiation force is small, and causes the weak directional removal of the aerosols between the node and anti-node, which constitutes the weak interaction. Conversely, the absolute dot causes the peak sound pressure at node to be low and the pressure gradient to be high. Therefore, the acoustic radiation force is great, which results in the strong interaction. Such strong interaction might cause the absolute removal of aerosols in region *X*.

Finally, in terms of region *X*, the characteristic length λ/2 of aerosol manipulation, showed in Fig. 3(a), equals to two times of the distance between the two positions of x_5 and x_6, showed in Fig. 5(a) & (b). Fig. 6 demonstrates a common characteristic length *a* to any ASW field. This characteristic length *a* is integer times of quarter-wavelength, and shows the distance of contiguous aerosol accumulation regions. There are rare aerosols in single region with length *a*. Hence, in NTASWF under π-mode phase the characteristic length *a* showed by Fig. 6 equals to λ/2. In one-dimensional ASW field, however, the characteristic length is only quarter-wavelength [9,17], that is, $a = \lambda/4$ in Fig. 6. For one dimension ASW field or its simplified analogy from higher dimension,

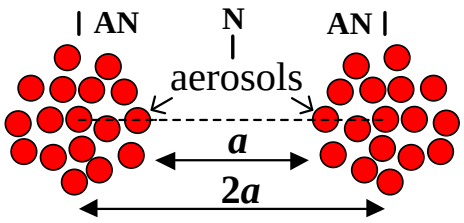

Fig. 6. Characteristic length between contiguous two anti-nodes.

the positions of antinodes and nodes demonstrate the tendency positions of accumulated aerosols driven by acoustic radiation force. The distance (one-wavelength) of contiguous antinodes for the NTASWF under π-mode phase is twice than the distance (half-wavelength) for the one dimension ASW field. Therefore, the characteristic length here under the π-mode phase is twice as much as that in the one-dimensional ASW field of the previous study [7,9,17]. According to the above analysis, the characteristic length increase is derived from the NTASWF under π-mode phase.

4. Conclusion

Acoustic tunable phase-control has been used successfully to manipulate the interaction between aerosols and NTASWF at resonant frequency 2.6427 kHz through a macro-scale modular platform. The specific acoustic field of aerosols regularly manipulated is assembled through this modular platform. The aerosols used are tobacco smoke. It was found that the suitable NTASWF was caused in the cavity and then NTASWF caused an X-pattern distribution for aerosols. Aerosols in cavity are divided into five regions by X-pattern. In the region X, the aerosols is rarer compared with the other regions. The major size of X-pattern under π-mode phase is 6.56 cm greater than 3.28 cm under 0-mode phase. The major areas to remove aerosols are 39 cm^2 (π-mode) and 9.7 cm^2 (0-mode). Acoustic tunable phase-control does change the distribution of sound pressure and regulate the structural factors of acoustic field. These factors are considered as the main intermediate variables for realizing the aerosol manipulation by acoustic tunable phase-control. It must be pointed that the degree of interaction between aerosols and acoustic field is decided by the shape of sound pressure nodes, that is, necks corresponding to weak interaction and dots corresponding to strong interaction.

The manipulation is effective at 298 K for the aerosols of the aerosol size distribution ranged in 0.08 μm–1 μm and of the aerosol concentration ranged in 51.6–93.3% (opacity).

Acknowledgements

The authors gratefully acknowledge the support for the National Nature Science Foundation of China (11190015, 51006023) and the Doctoral Program of Higher Education of China (20130092110007).

Appendix A

In order to demonstrate a good result on aerosol manipulation proposed in this paper, a chemical smog material is chosen as a different aerosol resource to display the manipulation effect. The main compounds of the material consist of tetramethrin, three chlorine permethrin. The size distribution of such aerosols corresponds to <1 μm (55.6% aerosols), 1–2.5 μm (37.5% aerosols), 2.5–4 μm (6.9% aerosols), which measured by Dust Track II-Model 8532. A similar result is caused and showed in Fig. A.1.

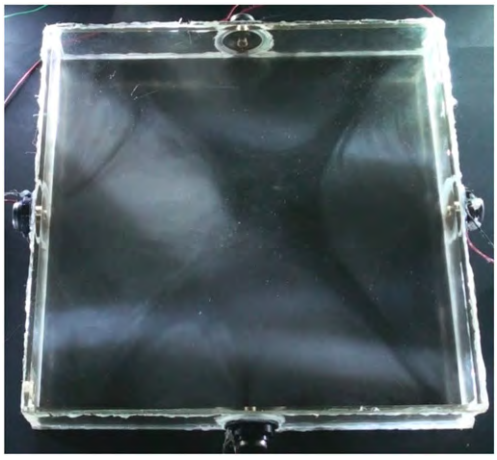

Fig. A.1. Aerosol manipulation for a chemical smog material under π-mode phase.

References

[1] J.Z. Liu, G.X. Zhang, J.H. Zhou, J. Wang, W.D. Zhao, K.F. Cen, Experimental study of acoustic agglomeration of coal-fired fly ash particles at low frequencies, Powder Technol. 193 (2009) 20–25.

[2] J.Z. Liu, J. Wang, G.X. Zhang, J.H. Zhou, K.F. Cen, Frequency comparative study of coal-fired fly ash acoustic agglomeration, J. Environ. Sci. 23 (2011) 1845–1851.

[3] Q.J. Guo, Z.N. Yang, J.S. Zhang, Influence of a combined external field on the agglomeration of inhalable particles from a coal combustion plant, Powder Technol. 227 (2012) 67–73.

[4] J.A. Gallego-Juarez, E. De Sarabia, G. Rodriguez-Corral, T.L. Hoffmann, J.C. Galvez-Moraleda, J.J. Rodriguez-Maroto, et al., Application of acoustic agglomeration to reduce fine particle emissions from coal combustion plants, Environ. Sci. Technol. 33 (1999) 3843–3849.

[5] W.T. Yuen, S.C. Fu, J.K.C. Kwan, C.Y.H. Chao, The use of nonlinear acoustics as an energy efficient technique for aerosol removal, Aerosp. Sci. Technol. (2014) 907–915.

[6] J. Greenhall, F.G. Vasquez, B. Raeymaekers, Continuous and unconstrained manipulation of micro-particles using phase-control of bulk acoustic waves, Appl. Phys. Lett. 103 (2013) 074103.

[7] N.D. Orloff, J.R. Dennis, M. Cecchini, E. Schonbrun, E. Rocas, Y. Wang, et al., Manipulating particle trajectories with phase-control in surface acoustic wave microfluidics, Biomicrofluidics 5 (2011) 044107.

[8] B. Raeymaekers, C. Pantea, D.N. Sinha, Manipulation of diamond nanoparticles using bulk acoustic waves, J. Appl. Phys. 109 (2011) 014317.

[9] D. Karpul, J. Tapson, M. Rapson, A. Jongens, G. Cohen, Limiting factors in acoustic separation of carbon particles in air, J. Acoust. Soc. Am. 127 (2010) 2153–2158.

[10] J.K.R. Weber, C.A. Rey, J. Neuefeind, C.J. Benmore, Acoustic levitator for structure measurements on low temperature liquid droplets, Rev. Sci. Instrum. 80 (2009) 083904.

[11] D. Foresti, G. Sambatakakis, S. Bottan, D. Poulikakos, Morphing surfaces enable acoustophoretic contactless transport of ultrahigh-density matter in air, Sci. Rep. 3 (2013) 3176.

[12] D. Foresti, M. Nabavi, D. Poulikakos, On the acoustic levitation stability behaviour of spherical and ellipsoidal particles, J. Fluid Mech. 709 (2012) 581–592.

[13] Q. Yao, S.Q. Li, H.W. Xu, J.K. Zhuo, Q. Song, Reprint of: Studies on formation and control of combustion particulate matter in China: a review, Energy 35 (2010) 4480–4493.

[14] D.S. Sun, X.D. Zhang, L. Fang, Coupling effect of gas jet and acoustic wave on inhalable particle agglomeration, J. Aerosol Sci. 66 (2013) 12–23.

[15] D.S. Scott, A new approach to acoustic conditioning of industrial aerosol emissions, J. Sound Vib. 43 (1975) 607–619.

[16] Z. Qiao, Y. Huang, W. Dong, Acoustic resonance characteristics of symmetric cylindrical waveguide with Helmholtz sound source, J. Southwest Univ. National. (Nat. Sci. Ed.) 44 (2014) 579–584 (In Chinese).

[17] L. Johansson, M. Evander, T. Lilliehorn, M. Almqvist, J. Nilsson, T. Laurell, et al., Temperature and trapping characterization of an acoustic trap with miniaturized integrated transducers — towards in-trap temperature regulation, Ultrasonics 53 (2013) 1020–1032.

[18] R.R. Boullosa, F. Orduna-Bustamante, Acoustic levitation at very low frequencies, Acta Acust. Acust. 96 (2010) 376–382.

[19] D.Y. Ma, Helmholtz resonator, Tech. Acoust. (Shanghai, P.R.C.) 21 (2002) 2–3 (In Chinese).

[20] K. Jia, K. Yang, D. Mei, Quantitative trap and long range transportation of micro-particles by using phase controllable acoustic wave, J. Appl. Phys. 112 (2012) 054908.

[21] T. Kozuka, T. Tuziuti, H. Mitome, F. Arai, T. Fukuda, Three-dimensional acoustic micromanipulation using four ultrasonic transducers, MHS 2000: Proceedings of the 2000 International Symposium on Micromechatronics and Human Science 2000, pp. 201–206.

[22] M.H. Becquemin, J.F. Bertholon, M. Attoui, F. Roy, M. Roy, B. Dautzenberg, Particle size in the smoke produced by six different types of cigarette, Rev. Mal. Respir. 24 (2007) 845–852.

[23] W.D. Van Dijk, R. Cremers, W. Klerx, T.R.J. Schermer, P.T.J. Scheepers, Application of cigarette smoke characterisation based on optical aerosol spectrometry. Dynamics and comparisons with tar values, Curr. Anal. Chem. 8 (2012) 344–350.

[24] P.S. Christensen, S. Wedel, H. Livbjerg, The kinetics of the photolytic production of aerosols from SO_2 and NH_3 in humid air, Chem. Eng. Sci. 49 (1994) 4605–4614.

[25] M.S. Kumar, A. Kerihuel, J. Bellettre, M. Tazerout, Experimental investigations on the use of preheated animal fat as fuel in a compression ignition engine, Renew. Energy 30 (2005) 1443–1456.

[26] J. Sae, Recommended practice, Snap acceleration smoke test procedure for heavy-duty powered vehicles, Society of Automotive Engineers, 1996. 1996–2002.

[27] X.Y. Ding, S. Lin, B. Kiraly, H.J. Yue, S.X. Li, I.K. Chiang, et al., On-chip manipulation of single microparticles, cells, and organisms using surface acoustic waves, Proc. Natl. Acad. Sci. U. S. A. 109 (2012) 11105–11109.

[28] L. Gor'Kov, On the forces acting on a small particle in an acoustical field in an ideal fluid, Sov. Phys. Dokl. 6 (1962) 773–775.

[29] M. Groschl, Ultrasonic separation of suspended particles — part I: fundamentals, Acustica 84 (1998) 432–447.

[30] G. Whitworth, W.T. Coakley, Particle column formation in a stationary ultrasonic-field, J. Acoust. Soc. Am. 91 (1992) 79–85.

[31] L.V. King, On the acoustic radiation pressure on spheres, Proc. R. Soc. A-Math. Phys. Eng. Sci. 147 (1934) 212–240.

[32] A.R. Noorpoor, A. Sadighzadeh, H. Habibnejad, Experimental study on diesel exhaust particles agglomeration using acoustic waves, Int. J. Automot. Eng. 2 (2012) 252–260.

[33] I. Buttinoni, G. Volpe, F. Kuemmel, G. Volpe, C. Bechinger, Active Brownian motion tunable by light, J. Phys. Condens. Matter 24 (2012) 284129.

[34] M. Alonso, Y. Endo, Dispersion of aerosol particles undergoing Brownian motion, J. Phys. A Math. Gen. 34 (2001) 10745–10755.

[35] R.L. Saxton, W.E. Ranz, Thermal force on an aerosol particle in a temperature gradient, J. Appl. Phys. 23 (1952) 917–923.

[36] A. Grinenko, C.K. Ong, C.R.P. Courtney, P.D. Wilcox, B.W. Drinkwater, Efficient counter-propagating wave acoustic micro-particle manipulation, Appl. Phys. Lett. 101 (2012) 233501.